Effect of Taylor Vortices on Mass Transfer from a Rotating Cylinder

R. Srinivasan, S. Jayanti and A. Kannan
Dept. of Chemical Engineering, IIT-Madras, Chennai 600 036, India

DOI 10.1002/aic.10553
Published online August 8, 2005 in Wiley InterScience (www.interscience.wiley.com).

Mass transfer from solids, which has important applications in a number of chemical and pharmaceutical industries, has been studied experimentally and semiempirically under turbulent flow conditions, and correlations are available in the literature to calculate the mass-transfer coefficients from pellets, rotating cylinders and disks etc. However, mass transfer under laminar flow has not been sufficiently addressed. One of the difficulties here is the strong Reynolds number dependence of the flow pattern, for example, due to the onset of Taylor vortices for the case of a rotating cylinder. This problem is circumvented by using a computational fluid dynamics (CFD)-based solution of the governing equations for the case of a cylinder rotating inside a stationary cylindrical outer vessel filled with liquid. The parameters cover a range of Reynolds number (based on the cylinder diameter, and the tangential speed of the cylinder), Schmidt number and the ratio of the outer to inner cylinder diameters. The results confirm that the circumferential velocity profile is a strong function of the Reynolds number and varies from a nearly Couette-type flow at very low Reynolds numbers to a boundary layer-like profile at high Reynolds numbers. The onset of Taylor vortices has a strong effect on the flow field and the mass-transfer mode. The calculations show that the Sherwood number has a linear dependence on the Reynolds number in the Couette-flow regime, and roughly square-root dependence after the onset of Taylor vortices. Correlations have been proposed to calculate the Sherwood number taking account of these effects. © 2005 American Institute of Chemical Engineers *AIChE J,* 51: 2885–2898, 2005
Keywords: CFD, solid dissolution, mass transfer, Taylor vortices, rotating cylinder, laminar flow

Introduction

Dissolution of solid materials in liquids finds wide-spread applications in the chemical process industries. Knowledge of the mass-transfer rates between a solid and an agitated liquid in a vessel is of considerable importance in the design of units, such as crystallizers, stirred-tank reactors for diffusion controlled solid-fluid reactions, and units involving physical dissolution. Some industrial examples of solid dissolution process are:

- Dissolution of metals, such as tin, lead and zinc in heat exchange media, such as mercury and sodium at high-temperatures, and their deposition at lower temperatures.[1]
- Limestone dissolution in an aqueous solution which is a phenomenon of interest in liming of acid lakes, flue gas desulfurization.
- The sustained drug delivery process in pharmaceutical applications which is determined by the rate of solid dissolution in the liquid medium.
- Mass transfer from a rotating cylinder which is of practical importance in electrochemical processes, such as electrodeposition, coating and metal recovery.[2]
- Recent application of mass transfer from rotating cylin-

Correspondence concerning this article should be addressed to S. Jayanti at sjayanti@iitm.ac.in.

ders in filtration and reverse osmosis processes where Taylor vortices (see later) are induced to enhance the mass-transfer rates.

Dissolution of solids has been extensively studied from both theoretical and experimental fronts. Three idealized configurations of the solid, namely, suspended pellets, rotating disk and rotating cylinder, have been considered in the literature. Eisenberg et al.[3] reported on one of the first systematic studies of solid dissolution from a rotating cylinder over a wide range of Reynolds and Schmidt numbers. Johnson and Huang[4] studied the rates of dissolution of organic solid from a flat surface into a turbulent liquid in an agitated vessel. Bennett and Lewis[1] made a comparison between the dissolution of lead and tin in mercury with the dissolution of benzoic acid in water, and found that the metal dissolution rates were transport controlled. Sherwood and Ryan[5] studied experimentally the mass transfer with and without chemical reaction from rotating benzoic acid cylinders. Marangozis and Johnson[6] reviewed solid dissolution data of suspended pellets, flat disks and rotating cylinders, and recommended cube-root dependency of the Sherwood number on the Schmidt number. Studies on solid-liquid mass transfer have been reviewed extensively by Pangarkar et al.[7]

There have been a number of more recent studies of mass transfer from a rotating cylinder with and without axial flow.[8,9,10,11,12,13,14,15] The configurations studied include cases with inner cylinder alone rotating and outer cylinder alone rotating, and are spread over large ranges of Reynolds and Taylor and Schmidt numbers. Most of these have been experimental studies and do not include detailed measurement of the flow field. An important aspect of mass transfer from a rotating cylinder is the possibility of occurrence of Taylor vortices.[16,17] The rotational motion of the inner cylinder (Taylor vortices do not occur when the outer cylinder alone rotates) induces a primarily circumferential flow in the annular region between the inner and the outer cylinders. If the rotational speed is sufficiently high (but not too high), then large-scale secondary flows, typically of the size of the gap width as shown in Figure 1a, are formed. It is to be expected that the presence of these Taylor vortices has a strong effect on the mass-transfer rate from the cylinder. While this flow situation has been widely investigated for very small gap widths in connection with the stability of the flow, there have been relatively few studies of the mass transfer, and also of the flow field for large gap widths typically used in mass transfer applications. In a recent study, Baier et al.[15] used computational fluid dynamics (CFD) simulations to obtain the velocity field for the case of the inner cylinder rotating, and used a boundary layer approximation to study the mass transfer aspects for small values of Taylor numbers. They found that the mass-transfer coefficient in the presence of the Taylor vortices varied as $Sh \sim Re^{0.46}$, which agreed with the experimental results of Coeuret and Legrand,[11] Holeschovsky and Cooney[14] who studied for the case of no axial flow and inner cylinder rotating, and also with the results of Kataoka et al.[9] who investigated the case of the outer cylinder rotating. Earlier, Kawase and Ulbrecht[13] used an analogy with the secondary flow in helical coils to arrive at the same result. Experiments at high Taylor numbers[3,12] show a stronger dependence of the Sherwood number on the Reynolds number with the exponent being in the range of 0.6 to 0.72.

Thus, there is considerable literature on the mass transfer from rotating cylinders. However, a detailed description of the flow field within the annular region is absent in these studies, presumably due to the nontrivial dependence of the velocity field on the Reynolds number and the radii of the inner and outer cylinders, among other parameters. Baier et al.[15] who included some of these effects in their computation of the velocity field, used a boundary layer analogy for mass transfer. Thus, their study is not applicable for very low Taylor numbers. In this article, we take advantage of the accuracy—for laminar flow simulations—offered by computational fluid dynamics (CFD) techniques to simulate the complete problem, that is, calculate both the velocity field and the scalar concentration field, for a range of flow conditions including very low Taylor numbers where Taylor vortices are not present. The simulations cover a range of Reynolds numbers, diameter ratios and height to diameter ratios of the cylinders. Results from these simulations show clearly the marked change in the mass-transfer coefficient upon the onset of Taylor vortices. Details of the calculation methodology, and the results obtained are discussed later.

Problem Formulation and Calculation Methodology

Governing equations for fluid flow

The equations solved for a CFD solution are the continuity and the momentum equation, which can be written as follows using vector notation:

Continuity equation: for an incompressible Newtonian fluid

$$\nabla \cdot \mathbf{u} = 0 \tag{1}$$

Momentum equation

$$\frac{\partial \mathbf{u}}{\partial t} + (\nabla \cdot \mathbf{u}\mathbf{u}) = -\frac{1}{\rho}\nabla p + \nu \nabla^2 \mathbf{u} \tag{2}$$

Here u is the velocity; p is the static pressure, ρ is the density, and ν is the kinematic viscosity. Since the fluid under consideration is a liquid and the velocities are small, a constant-property fluid assumption is made.

The mass concentration of the dissolving substance is calculated by solving the following generalized scalar transport equation

$$\frac{\partial}{\partial t} Y_A + (\nabla \cdot \mathbf{u} Y_A) = \frac{1}{\rho} \nabla \cdot (\Gamma_{AB} \nabla Y_A) \tag{3}$$

where Y_A is the mass fraction of the scalar A, that is, the mass of the scalar per total mass in the control volume. Γ_{AB} is the molecular diffusivity (in kg/ms) of the scalar in the liquid B, defined as $\Gamma_{AB} = \rho D_{AB}$, where D_{AB} is the kinematic molecular diffusivity in m^2/s. This approach has previously been used by one of the authors,[18] to calculate the mixing time in jet-mixed vessels. The scalar is assumed to be a neutrally buoyant scalar so that the density and the viscosity of the fluid are unaffected by the scalar concentration. Since benzoic acid, the solid under consideration, is only sparingly soluble in water, the fluid under consideration, this is a reasonable assumption.

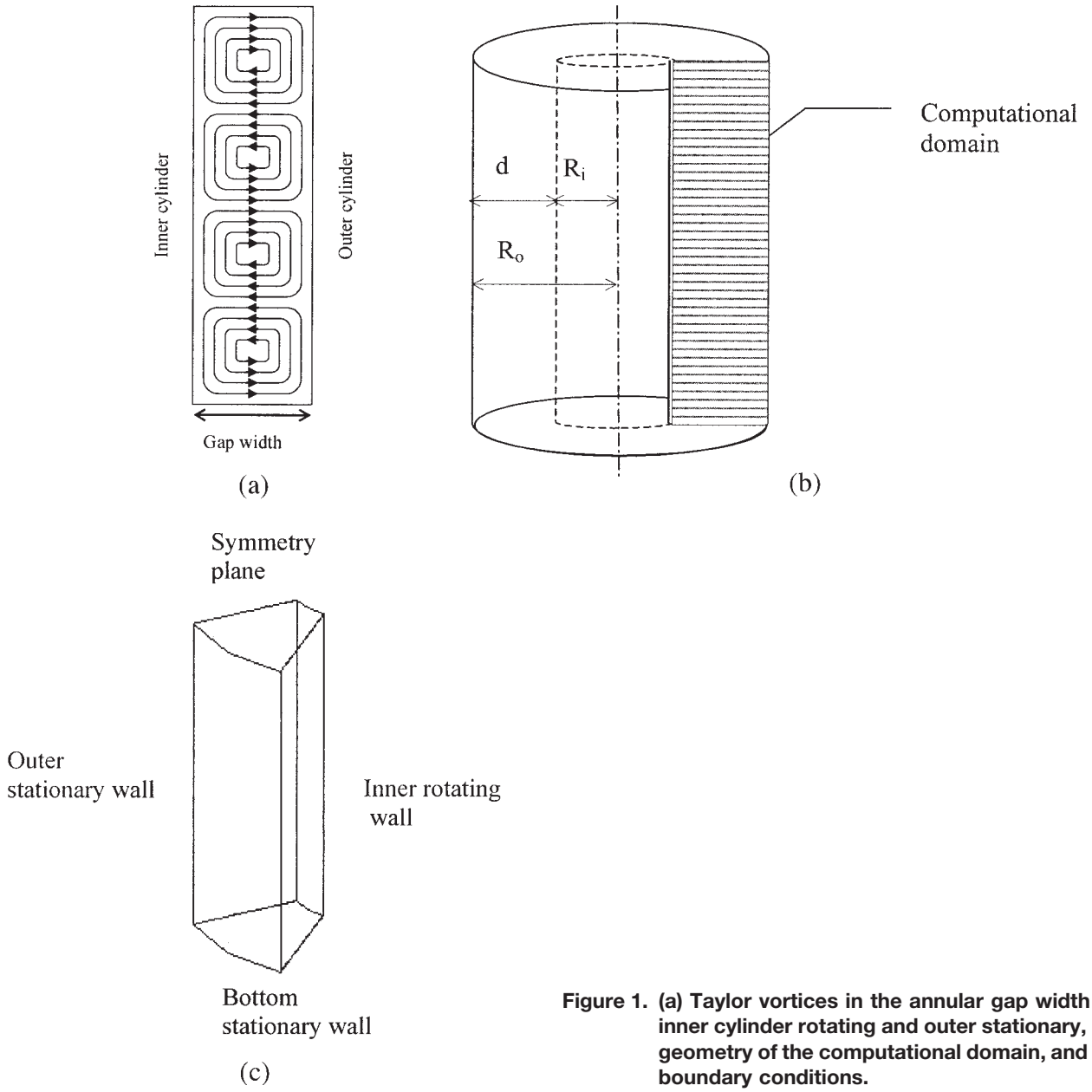

Figure 1. (a) Taylor vortices in the annular gap width of inner cylinder rotating and outer stationary, (b) geometry of the computational domain, and (c) boundary conditions.

Flow domain and boundary conditions

The flow domain consists of an inner rotating cylinder and an outer stationary cylindrical vessel filled with a liquid up to a given height. The inner solid cylinder is concentric with the axis of the vessel and rotates at a constant angular velocity. There are no internal parts, such as baffles in the vessel, and the problem is treated as being axisymmetric for the low Taylor numbers studied in this work. The flow domain consists of the liquid in the annular region between the inner rotating cylinder and the outer stationary cylinder, and is bounded at the bottom by a stationary wall and at the top by a planar shear-free interface, as shown in Figures 1b and 1c. The problem is formulated in cylindrical coordinates, the axial, radial and tangential velocity components being u, v, and w, respectively. No-slip boundary conditions are imposed on all walls. Thus, a constant tangential velocity is specified at the inner cylinder, and a zero velocity is specified on the outer wall and the bottom wall. A symmetry boundary condition is specified on the top wall to make it a zero-shear surface. Since the major flow is in the circumferential direction, all the three velocity components have to be resolved. For this reason, the flow in a 45° sector of the cylinder is simulated, and periodicity condition is imposed on the two bounding circumferential planes. For the mass fraction equation, a constant wall mass fraction, which is based on the solubility limit of benzoic acid in water, estimated to be 4.067×10^{-3} at a temperature of 30°C, is applied on the surface of the inner cylinder and a Neumann boundary condition (zero normal gradient) is applied on the other boundaries.

The solution of the coupled mass, momentum and mass-transfer equations has been done in two stages. In the first stage, the mass and the momentum equations are solved together under steady conditions to obtain the steady-state ve-

locity and pressure fields. In the second stage, the time-dependent mass fraction equation, which is coupled in a one-way mode to the mass and momentum equations, is solved with the velocity field obtained from the steady-state calculations as the initial condition for the velocity field. The mass fraction in the interior of the domain at the beginning of the calculation is assumed to be zero throughout.

Details of Numerical Solution

Computer code

All the calculations reported here have been carried out using the commercially available CFX 4.4 computer code developed by AEA Technology, UK. CFX is a general purpose computer program, which uses a finite volume method-based discretization of the governing partial-differential equations on a nonstaggered, structured, body-fitted grid. The chequer-board type of oscillations of pressure and velocity that are associated with the use of a nonstaggered grid are eliminated using the Rhie-Chow interpolation scheme[19] to estimate the face velocities. The pressure-velocity coupling for incompressible flows is effected using the SIMPLE family of schemes[20] adapted for a nonstaggered body-fitted grid.

Discretization schemes

The computer program has different discretization schemes for the user to choose from for a particular problem. In the present case, the convection terms in the governing flow equations have been discretized using the third-order accurate QUICK scheme,[21] while the diffusion terms have been discretized, using the second-order accurate central scheme. For the solution of the mass-fraction equation, it was found that using the QUICK scheme gave negative values of the mass fraction; hence, the SUPERBEE scheme,[22] which incorporates the total variation diminishing (TVD) property to eliminate oscillations associated with high order differencing schemes, has been used. The overall accuracy of the discretization can, therefore, be said to be of second-order.

Grids

The structured, orthogonal grid for the two-dimensional (2-D) flow domain consisted typically of 9,600 cells. For example, in the case with a cylinder height of 0.12 m, and a gap width of 0.035 m, a 100 $\times$ 96 nonuniform grid was used to discretize the 2-D flow domain in the x-r plane, x being axial direction, and r being radial direction. Since the precise location of the Taylor vortices was not known *a priori,* uniform grid spacing was used in the axial direction. In order to resolve the strong velocity and mass fraction gradients in the radial direction, an expanding grid was used. Preliminary calculations were made with different grids to check for grid independence of the results. The computed velocity profile near the inner cylinder was compared for three radial grids in which the grid spacing near the wall was successively reduced by a factor of two. Similarly, the grid independence in the axial direction was also verified by repeating the calculations with a grid spacing which is halved. The temporal discretization was also verified by calculating the mass-fraction equation with a series of decreasing time steps.

Formulation of the mass transfer problem

The problem under consideration is the determination of the mass-transfer coefficient from a rotating cylinder made of the solid to be dissolved. The specific case being studied is that of the dissolution of benzoic acid in water in which the former is sparingly soluble. Experimentally this is done by measuring the concentration of the benzoic acid in the solution as a function of time. It can be shown[4] that the cup mean concentration with time is given by the following expression

$$-\ln\left(1-\frac{C_A}{C_{AW}}\right)=(k_cS/V)t \tag{4}$$

where k_c is the mass-transfer coefficient, S is the surface area of the inner cylinder, V is the volume of the liquid, C_A is the bulk mean concentration at time t, C_{AW} is the solubility concentration of the solid in liquid. The mass-transfer coefficient is obtained from the slope by plotting LHS vs. time. In the present calculations, this is simulated by the numerical solution of the time-dependent transport equation of a passive, neutrally buoyant scalar (Eq. 3) with the appropriate diffusivity value and subject to initial and boundary conditions. (It is assumed that the dissolution rate is small enough that one does not have to consider the radial movement of the cylinder surface due to dissolution.) The mass-transfer coefficient can now be obtained in one of two ways: (1) by plotting the temporal variation of the cup mean concentration in the vessel, which gives the time-averaged mass-transfer coefficient, and (2) from the slope at the wall of the radial profile of the instantaneous mass fraction. It was found that the two gave nearly the same results; however, the computed temporal variation was not exactly linear, especially in the initial stages of the calculation. Hence, the second method was followed to determine the mass-transfer coefficient. Here, two additional complications arise in the evaluation of the mass-transfer coefficient. First, the mass-transfer rate is a function of the local velocity field and, therefore, shows axial variation when Taylor vortices are present. An axial average of the computed wall mass flux was, therefore, taken to smooth out these variations. Second, in many cases, especially at low rotational speeds, the mass-fraction profile did not have a clearly defined bulk concentration. Therefore a cup mean mass fraction, defined as follows

$$Y_c=\frac{\int_0^L\int_{R_i}^{R_0} w(r,x)Y(r,x)2\pi r\,dr\,dx}{\int_0^L\int_{R_i}^{R_0} w(r,x)2\pi r\,dr\,dx} \tag{5}$$

was used as the bulk mass fraction. The mass-transfer coefficient was then calculated as

$$k_c=\frac{j_A}{\rho(Y^*-Y_c)} \tag{6}$$

where j_A is the axially-averaged mass flux at the inner cylinder at a given time wall which is directly obtained from the computer program, Y^* is the wall mass fraction obtained from the solubility concentration of the solid in liquid and Y_c is the computed cup mean mass fraction in the vessel at that time. This is then converted into a Sherwood number based on hydraulic diameter as follows

$$Sh_{Dh} = \frac{k_c(2d)}{D_{AB}} \tag{7}$$

where d is the gap width.

Validation

It can be seen from the description of the earlier calculation methodology that the exact equations governing the flow are being solved. The major assumptions are the flow is laminar, axisymmetric, Newtonian with the fluid having constant physical properties, which are reasonable for the problem under consideration. Thus, unlike in turbulent flow calculations, there are no modeling assumptions as far as the equations are concerned. The principal sources of error, therefore, are the discretization of the equations and the boundary conditions. The former can be reduced by employing a fine grid, which has been verified by the grid independence tests. The no-slip boundary conditions on the walls require no validation; the imposition of a shear-free interface condition at the top surface limits the application to low-rotational speeds so that the interface remains flat. Finally, the assumption of axisymmetry is also a limiting condition, because it is expected that as the rotational speed increases, the axisymmetric Taylor vortices may become unstable giving rise to a wavy type of Taylor vortices.[23]

To demonstrate the validity of the simulations, results obtained from the present study are compared with theoretical results for the onset of Taylor vortices. This case is considered by a number of researchers. Among these, DiPrima et al[24] considered the effect of the ratio of the inner and outer cylinder radii on the stability of Couette flow to axisymmetric and nonaxisymmetric perturbations for the case where the outer cylinder is at rest. They found that the ratio of the inner to outer radii η, had a significant influence on the critical Reynolds and Taylor numbers, defined respectively as

$$Re_{crit} = \frac{\Omega R_i d}{\nu} \tag{8}$$

$$Ta_{crit} = \frac{2(1-\eta)\,Re_{crit}^{\,2}}{(1+\eta)} \tag{9}$$

for the Couette flow to Taylor vortex flow transition to occur. In this study, this theoretical dependence on the radius ratio is taken as a benchmark for the validation of the present calculation methodology. Accordingly, simulations were conducted for three radius ratios, η namely, 0.632, 0.462 and 0.300, over a range of Reynolds numbers (here, the outer radius is changed while keeping the inner cylinder radius constant). Typically, the results are as shown in Figure 2 where the streamfunction

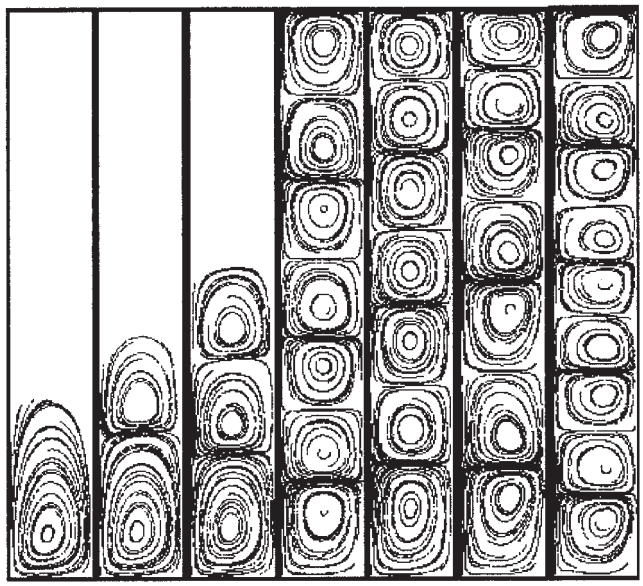

Figure 2. Streamfunction contours plotted in the annular region for different Reynolds number (Re_D) = 25, 60, 86, 127, 203, 456, 760 for the case of radius ratio (η) of 0.462.

contours are plotted in the annular region for different Reynolds numbers, based on inner cylinder diameter Re_D for the case of a radius ratio of 0.462. It can be seen that until the onset of the instability, no secondary flow is observed in the bulk of the annular region. (Since the bottom surface is a wall, this gives rise to a small amount of recirculation which cannot be associated with the Taylor vortex phenomenon; this recirculation is expected to disappear if the bottom surface too is made a shear-free surface.) Above a certain Reynolds number (or rotational speed for a given geometry), Taylor vortices appear all along the height of the annular region (see discussion on the effect of the height of the cylinder). This pattern is sustained at higher Reynolds numbers. Thus, for each radius ratio, a fairly demarcated Reynolds (or Taylor) number exists below which a Couette type of flow without significant secondary flow and above which Taylor cells are found over the entire domain. It should be noted that these flow patterns have been obtained by solving the steady state governing equations and, hence, they do not actually mimic the transition. The transitional Taylor numbers obtained from the present CFD simulations are compared in Figure 3, with the theoretical results obtained by DiPrima et al[24] for the three radius ratios. It can be seen that excellent agreement is obtained between the two.

Results from Numerical Simulations

Calculations of the solid dissolution process in a rotating cylinder have been made for several cases to investigate the effect of Reynolds number, Schmidt number and radius ratio. The diameter of the inner cylinder (D_i) is kept constant at 0.03 m in all cases, and three different outer diameters (D_o) 0.0475, 0.065 and 0.100 m were used to obtain radius ratios (η) of 0.632, 0.462 and 0.300, respectively. The height of the cylinder (L) was kept at 0.12 m in a majority of the cases; but some cases were repeated varied with twice the height to check

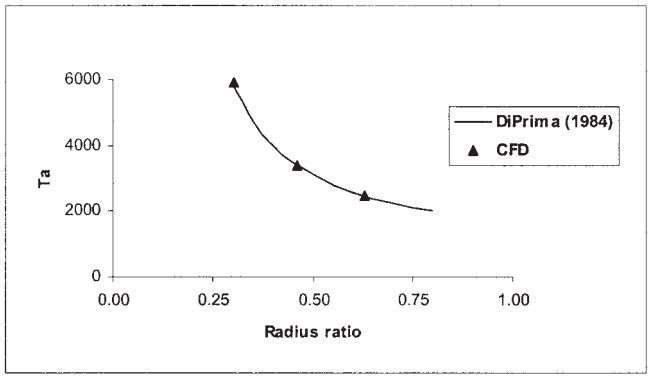

Figure 3. Transitional Taylor numbers obtained from the present CFD simulations compared with the theoretical results obtained by DiPrima et al[24] for the three radius ratios (η).

that the results were not dependent on the height of the domain. For the mass transfer cases, the base case corresponded to the estimated Schmidt number, *Sc*, of 877 for a benzoic acid-water system. Additional calculations were conducted by varying *Sc* in the range of 100 to 50,000 to determine the Schmidt number effect. The Reynolds number, based on the inner cylinder diameter and its surface speed, varied between 1 and 1,000. The results from these calculations are discussed later.

Typical velocity and mass fraction profiles

Owing to rotation of the inner cylinder, two distinct patterns of flow arise in the annular region in the range of parameters studied here. The changeover between these can be attributed to the onset of Taylor vortices. On the basis of the nature of the velocity field, these can be called as "Couette flow (shortened as *Couette flow*)" pattern and "Taylor vortex (shortened as *Taylor flow*) flow" pattern. Typical circumferential velocity profiles at midheight under these two conditions are shown in Figure 4a, for a radius ratio of 0.462, and a cylinder height to inner diameter of 4. The rotational speed of the inner cylinder is such that the Reynolds number, based on the inner cylinder diameter is 86 for the *Couette flow* case and 453 for the *Taylor flow* case. The velocity profiles are plotted in dimensionless form in which the circumferential velocity is divided by the surface speed ($=R_i\Omega$, where R_i is the radius of inner cylinder, and Ω is the angular velocity), and the radial distance from the wall of the inner cylinder is divided by the gap width. It can be seen that under *Couette flow* conditions, the velocity profile variation is nearly linear while under *Taylor flow* conditions, a more boundary layer-like velocity profile is obtained near the cylinder wall. The mass fractions corresponding to these two cases, for a Schmidt number of 877, are shown in Figure 4b (at a time corresponding to the same number of revolutions of the inner cylinder) in dimensionless form, in which the mass fraction is divided by the imposed mass fraction at the wall. Once again, a distinct, boundary layer type of variation is found under *Taylor flow* conditions while a nearly linear variation prevails under *Couette flow* conditions.

Taylor vortices introduce a convective element into the diffusion of the species from the dissolving wall into the bulk of the fluid. However, this convection is highly structured and helps only to some extent in the overall diffusion and dissolution of the substance. The final process of mixing and dissolution is still governed by molecular diffusion to the dissolving front and is a long process. This is summarized in Figure 5a, wherein the contours of mass fraction of the solute are shown in a single Taylor cell as a function of time for a radius ratio of 0.3, Reynolds number of 760 and Schmidt number of 877. In the initial period, there is rapid transport of the solute from the inner surface to the outer surface and back towards the inner surface, in a manner consistent with the streamline pattern. However, there is very little solute concentration in the "eye" of the vortex and further mixing of the solute in the core fluid

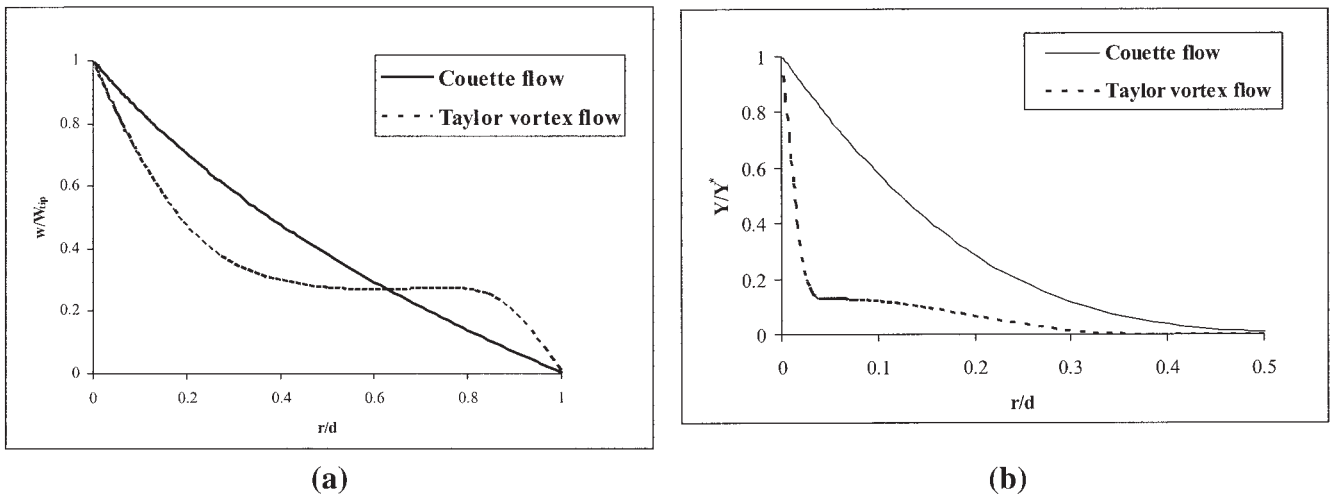

Figure 4. (a) Typical circumferential velocity profiles at midheight for a radius ratio of 0.462. Reynolds number (Re_D) is 86 for the *Couette flow* case, and 453 for the *Taylor flow* case. (b) Typical mass fraction profiles at midheight for a radius ratio of 0.462. Reynolds number (Re_D) is 86 for the *Couette flow* case, and 453 for the *Taylor flow* case.

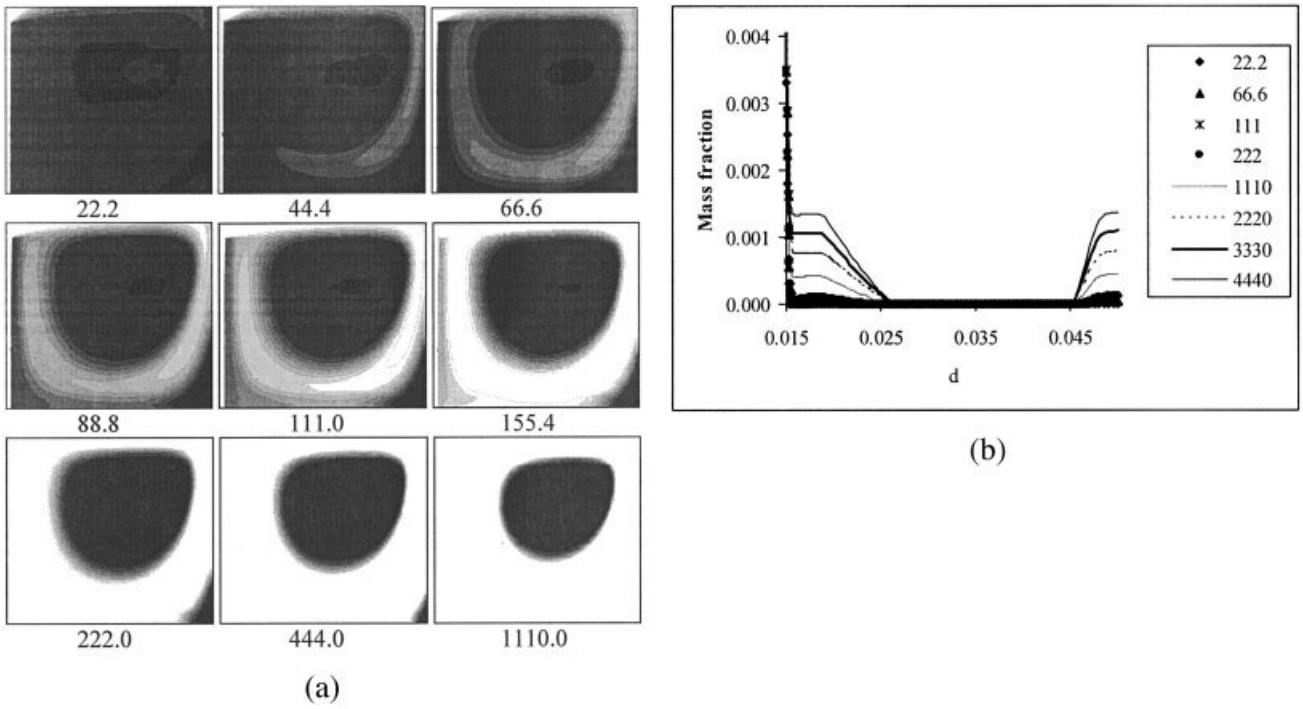

Figure 5. (a) Mass fraction contours within a single Taylor vortex cell, and (b) mass fraction profiles at midheight of the Taylor vortex cell at different times (s) for a radius ratio of 0.3, Re_D of 760 and *Sc* of 877.

is governed by the slow molecular diffusion process. This is illustrated in the gradual shrinking with time of the zero concentration region at the center of the vortex. The radial variation of the mass fraction along the centerline of the Taylor cell is shown in Figure 5b at different times for this case. The convective transport of the solute is effective in increasing the solute mass fraction near the inner and the outer walls. However, the concentration in the central part of the channel remains close to zero. Large mass fraction gradients exists between the central core and the well-mixed layer outside in the path of the convection currents. From this, it is clear that there is a relatively thin layer of well-mixed zone, and a large area of the unmixed core associated with each cell. Transport of the solute between these two zones is essentially by molecular diffusion and is, therefore, very slow.

Parametric Effects of *Re*, η, *L/D* and *Sc*

Effect of Reynolds number on Taylor vortices

The effect of Reynolds number variation on the overall flow pattern in the annular region can be seen in Figure 2, where the streamfunction contours are shown at different Reynolds numbers for a gap width of 0.0175 m. As mentioned earlier, Taylor vortices are formed only after a critical Taylor number. Further increase in the Taylor number leads to some distortion of the Taylor vortices; however, their number remains constant. A comparison of the radial profiles of the tangential velocity component at midheight is shown in Figure 6a in dimensionless form. Until the onset of Taylor vortices, all dimensionless profiles collapse onto a single curve (Figure 6a shows the velocity profiles for *Re* of 25 and 86 falling on the same, nearly Couette-type profile). As *Re* increases further, there is a gradual deviation from this, and a boundary layer type of variation is established at a Reynolds number of about 200. Further increase in *Re* makes the boundary layer-type variation more pronounced. It should be noted that the plots are all at midheight, and that there is some asymmetry in the Taylor vortex pattern, presumably due to the asymmetric boundary conditions at the top and the bottom of the annular region. Thus, the midheight location does not correspond to the same location relative to a Taylor vortex, and this adds a bit of uncertainty to the comparison of the velocity profiles at different Re_D. (This uncertainty is not in locating the midheight of the cylinder, but in being able to impose the conditions that the midheight of the cylinder always coincides with the midheight of the Taylor cell for all Reynolds numbers.) However, the transition to a boundary layer type velocity profile at high *Re* is unmistakable. The mass fraction profiles for different Reynolds numbers at a Schmidt number of 877 are shown in Figure 6b. These also show the Couette-type and boundary layer-type variations at low and high Reynolds numbers, respectively.

Effect of radius ratio

The effect of radius ratio on the dimensionless velocity profiles is summarized in Figure 7a and Figure 7b. Here the dimensionless tangential velocity is plotted in terms of dimensionless radial distance for three radius ratios, namely, 0.632, 0.462, 0.300 at a Reynolds number of 76 (Figure 7a), which corresponds to the *Couette flow* condition, and at a Reynolds number of 760 (Figure 7b), which corresponds to the *Taylor flow* condition. From Figure 7a, we note that, for small gap widths or high values of η, the radial profile of the circumferential velocity is nearly linear. As η decreases, the velocity profile becomes nonlinear, though monotonically decreasing. In the *Taylor flow* condition also (Figure 7b) the radius ratio

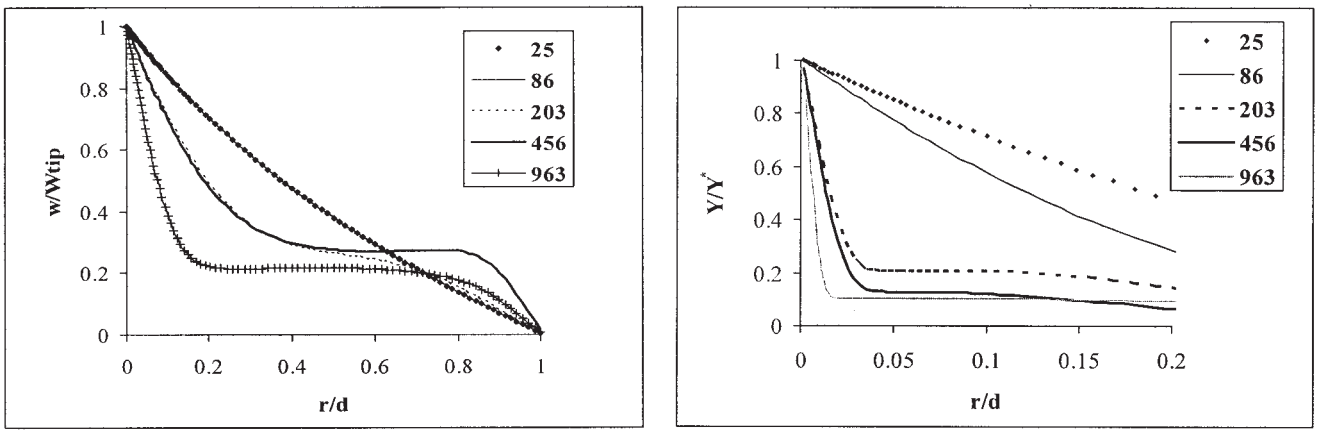

Figure 6. (a) Circumferential velocity profiles at midheight for a radius ratio of 0.462 for different Reynolds number (Re_D). (b) Mass fraction profiles at midheight for a radius ratio of 0.462 for different Reynolds number (Re_D).

has a significant effect on the tangential velocity profile. It is, therefore, to be expected that the radius ratio will have some parametric influence on the mass-transfer coefficient. Many existing correlations[1,6,25] for mass-transfer coefficient do not consider this factor.

Effect of the Schmidt number

The effect of Schmidt number on the mass fraction profiles is investigated by carrying out calculations in the *Sc* number range of 100 to 50,000. The *Sc* for the reference case of benzoic acid-water system is 877. It varies between 600 and 1,500 for other typical systems such as salicylic acid-water and 2-naphtol-water systems.[25] For metals, such as tin, lead and zinc dissolving in liquid metals, such as mercury, the Schmidt number is in the range[1] of 50 to 100, while for systems such as benzoic acid-sucrose solution, and benzoic acid-aqueous glycerol solution, it can vary in the range[8] of 3,000 to 40,000. The effect of this large variation of *Sc* on the mass fraction profile is summarized in Figure 8, where the concentration profiles are shown for different *Sc* at a Reynolds number of 76 (Figure 8a), and 760 (Figure 8b). The effect of increasing *Sc* is to decrease the rate of diffusion of the wall-imposed mass fraction. This effect predominates at low *Re*, and the Schmidt number is seen to have a large effect on the mass fraction profile. At high *Re*, the large convective diffusion caused by the Taylor vortices restricts the mass fraction variation to close to the walls (Figure 8b (1)). However, on a magnified scale (the profiles are redrawn in Figure 8b (2) over a dimensionless radial distance of 0.01), the effect of *Sc* on the mass fraction profiles is nearly the same as at low *Re*. Thus, the effect of *Sc* on the mass-transfer coefficient scales independently of Reynolds number, as will be shown later.

Effect of L/D

It is obvious that the height of the cylinder has little effect on the overall mass-transfer coefficient under *Couette flow* conditions as there is nearly no axial variation of the mass flux. However, the situation is different under *Taylor flow* condi-

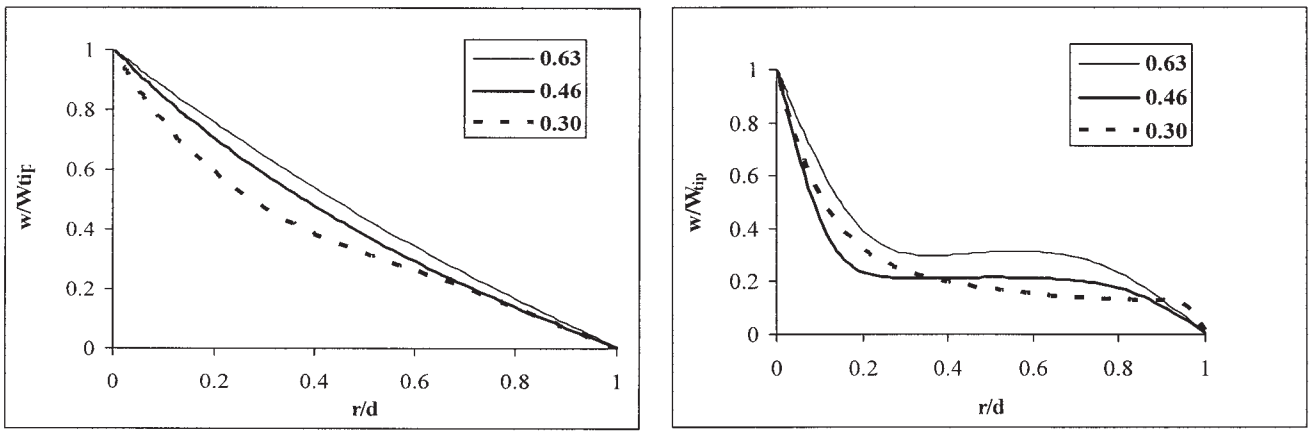

Figure 7. (a) Tangential velocity profiles for three different radius ratios (η) at Re_D = 76 (*Couette flow* condition). (b) Tangential velocity profiles for three radius ratios at Re_D = 760 (*Taylor flow* condition).

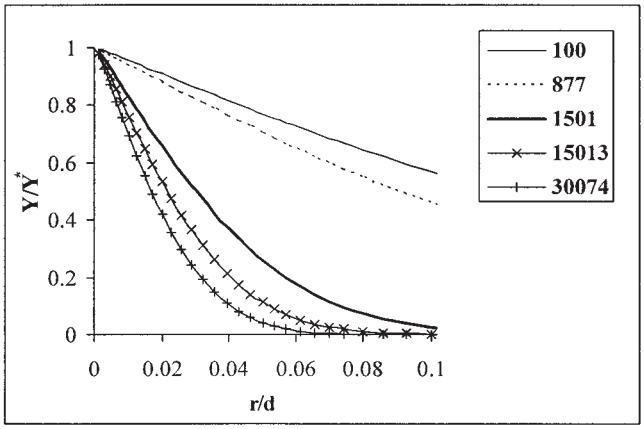

(a)

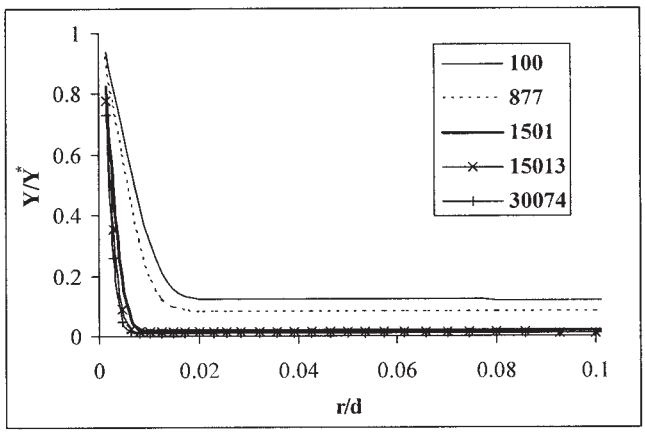

(b1)

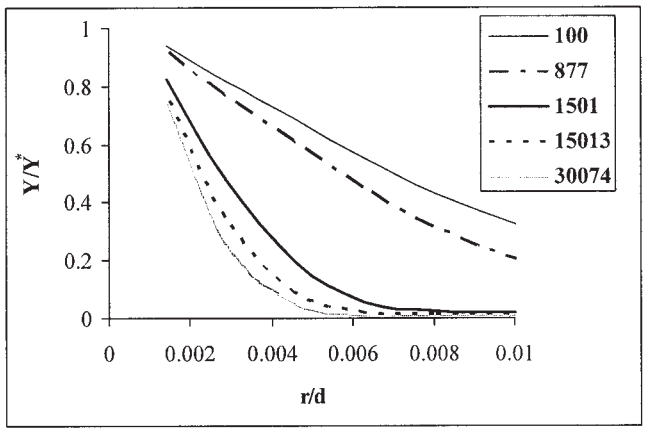

(b2)

Figure 8. (a) Effect of *Sc* on the mass fraction profile at a $Re_D = 76$ (*Couette flow* condition). (b) Effect of *Sc* on the mass fraction profile at a $Re_D = 760$ (*Taylor flow* condition).

tions. Typically, a number of Taylor cells are set up if the cylinder height is long enough. This can be seen in Figure 9a, where the streamfunction contours for a radius ratio of 0.30 are shown at a Reynolds number of 760. It can be seen that a number of Taylor cells, four in this case, are established and that the flow pattern is fairly regular. The circulation within one Taylor cell is shown in Figure 9b in the form of vector plot. The corresponding wall mass flux variation along the height is shown in Figure 9c, for a Schmidt number of 877 for two different heights. (Such strong periodic variation in the local mass-transfer coefficient has also been recorded experimentally by Kataoka et al[9]). This shows that except close to the bottom wall, a periodic mass flux variation, consistent with the Taylor cell pattern, is obtained on the inner cylinder surface. Thus, for a long enough height, a repeating pattern is obtained. However, if the cylinder height is less, as in the base case of a height of 0.12 m, and an inner cylinder dia. of 0.03 m (both these dimensions correspond to the experimental conditions of Sherwood and Ryan[5]), it is possible that the L/D ratio has an effect on the Taylor cell pattern. In order to investigate this, some calculations have been for twice the base case cylinder height of 0.12 m. The resulting axial mass flux variation is compared in Figure 8c for a Reynolds number of 760, and a Schmidt number of 877. It can be seen that the mass flux variation for the shorter cylinder case overlaps that for the longer cylinder case. Calculations with a wider gap show, however, that the predicted pattern may be affected if the gap width is increased by a factor of two while keeping the same height. These calculations show that the minimum height of the cylinder should be so as to allow a couple of Taylor cells to be resolved. Since the cell height is typically about the same as the gap width (see Figure 2), it can be concluded that the effect of liquid height would not be significant if $L/d > 2$.

Correlation for Mass-Transfer Coefficient

The calculation of the mass concentration profile enables the determination of the mass flux from the surface of the inner cylinder as

$$j_A = -\Gamma_{AB} \left. \frac{dY_A}{dr} \right|_{r=R_i} \tag{10}$$

The mass-transfer coefficient k_c, can then be evaluated as

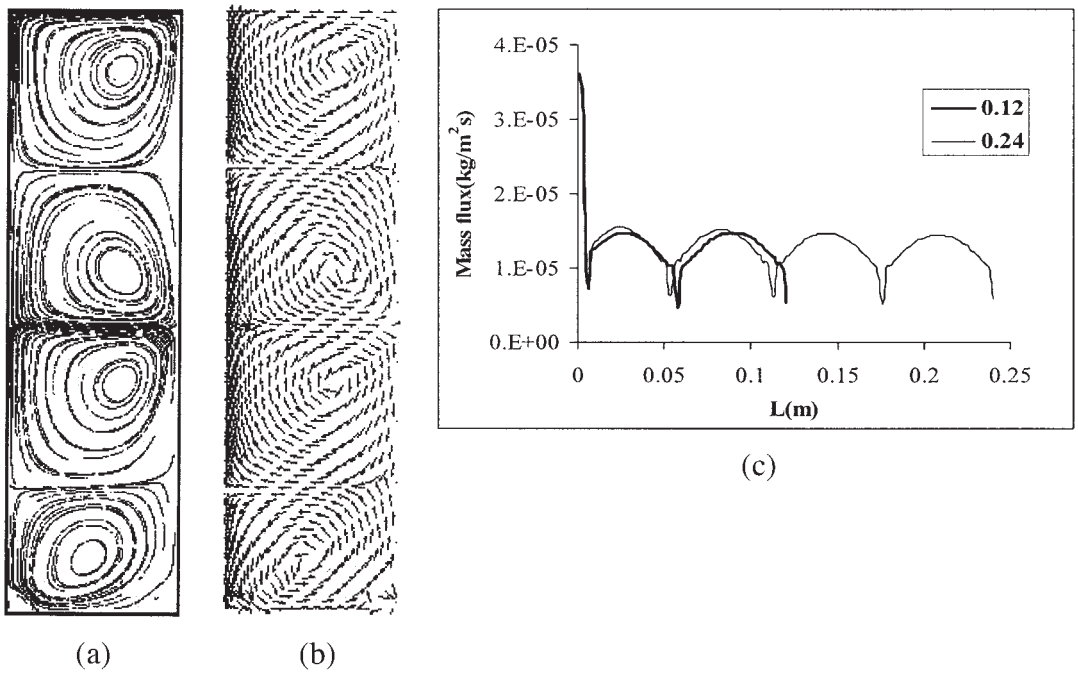

Figure 9. (a) Streamfunction contours for $\eta = 0.30$ at $Re_D = 760$. (b) Circulation within one Taylor cell in the form of vector plot. (c) Axial wall mass flux variation for two different heights at $Sc = 877$ and $Re_D = 760$.

$$k_c = \frac{j_A}{\rho(Y^* - Y_c)} \tag{11}$$

where Y^* is the imposed mass fraction at the inner cylinder, and Y_c is the mixed cup mean mass fraction defined in Eq. 5. The introduction of Y_c, the cup mean value of the mass fraction, is done for two reasons. First, because of the finite size of the annular region, the concentration at large r is not zero and increases with time. Second, Y_c is the desired parameter from a practical point of view as one can use it to determine how long the rotating cylinder has to be kept immersed in the solution for a specified amount of dissolution.

The presence of Taylor vortices makes the mass flux vary axially, typically as shown in Figure 9c. An axially averaged value of the mass flux is, therefore, taken to compute the mass-transfer coefficient. This is then converted into a Sherwood number, based on the hydraulic diameter as in Eq. 7. It should be noted that the gap width d here is one half of the hydraulic diameter for the same configuration. Thus, other definitions of Sherwood number, for example, based on the inner cylinder diameter or gap width are possible. The present definition is justified by the fact the Taylor number and the Reynolds number describing the flow are better with hydraulic diameter than on the diameter.

Typical variation of the computed Sherwood number with the Reynolds number is plotted in Figure 10 for the three

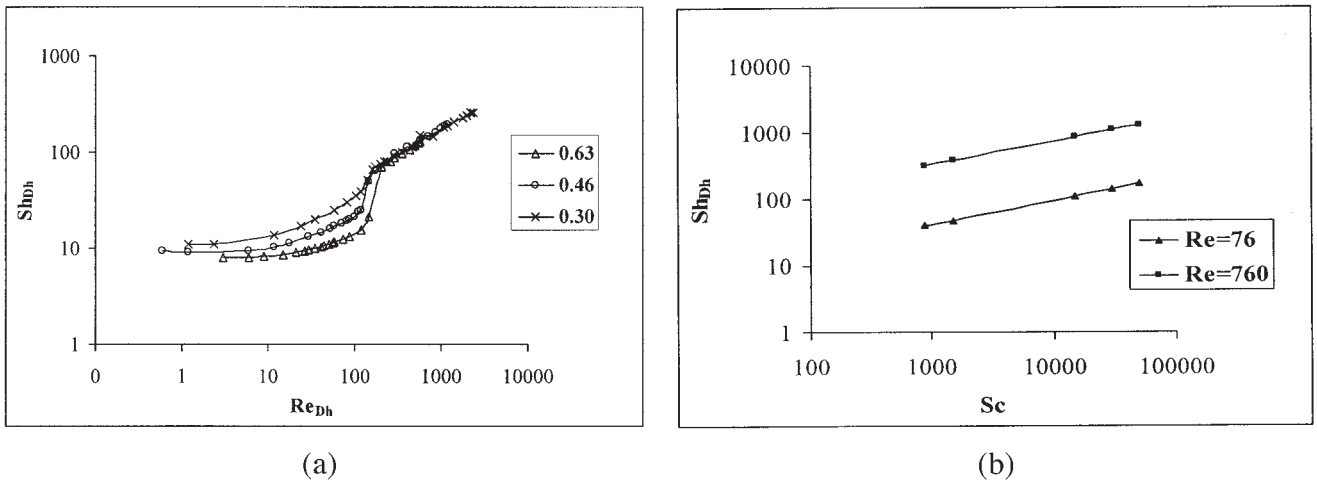

Figure 10. Sherwood number (Sh_{Dh}) variation (a) with Reynolds number (Re_{Dh}) for three radius ratios (η), and (b) with Schmidt number at $Re_D = 76$ (*Couette flow* region) and 760 (*Taylor flow* region).

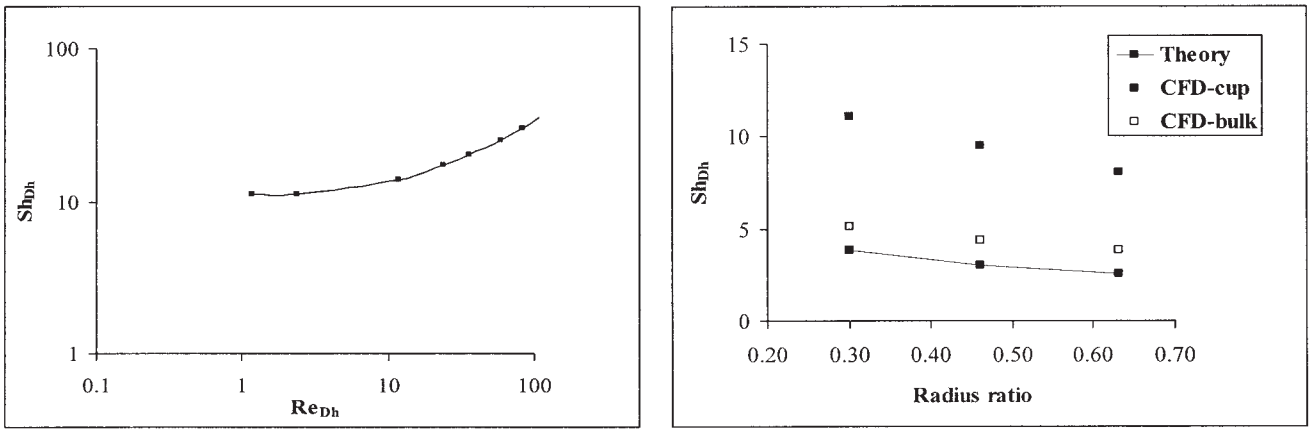

Figure 11. (a) Computed variation of Sh_{Dh} with Re_{Dh} for very low rotational speeds for $\eta = 0.3$. (b) Comparison of numerically obtained Sherwood number limiting values with that of CFD.

different radius ratios under consideration. The three curves more or less merge in the *Taylor flow* region, but differ significantly in the *Couette flow* region. Closer examination of the results shows that the variation of Sh with Re is typically linear in the *Couette flow* region, and that it exhibits a square-root variation in the *Taylor flow* region, that is, $Sh \sim Re^{0.5}$. While the variation in the *Couette flow* region has not been reported hitherto, a number of authors have reported a near-square root variation with Reynolds number, as mentioned earlier. The reason for this different behavior lies in the flow field. In the *Couette flow* region, the Couette-flow type of flow field gives rise to a linear variation. In the *Taylor flow* region, the dominant feature of the flow is the boundary layer type variation near the wall. Since the boundary layer thickness in laminar flow typically varies as $Re^{-0.5}$, the Sherwood number also varies as $Re^{1/2}$. The effect of Schmidt number on the Sherwood number is shown in Figure 10c at a Reynolds number of 76 and 760, corresponding, respectively, to the *Couette flow* and *Taylor flow* regions. It is seen that over the entire of Sc of between 100 and 50,000, Sh varies typically as $Sc^{1/3}$ in both the regions.

Finally, the limiting value of the Sherwood number at very low Reynolds numbers is of interest. For mass transfer from a stationary sphere, it can be shown that the Sherwood number under stagnant conditions[26] is 2. A similar analysis can be carried out for a stationary cylinder. The mass flux through a cylindrical plane at a radial distance of r under steady conditions, can be written as

$$-\frac{1}{r}\frac{\partial}{\partial r}(rN_{AR}) = 0 \tag{12}$$

where N_{AR} is the mass flux per unit area. Integrating Eq. 12, we get the radial variation of concentration as

$$C_A = C_1 \ln r + C_2 \tag{13}$$

Applying the boundary conditions that at $r = R_i$, $C_A = C_{AW}$, and that at $r = R_o$, $C_A = 0$, the two constants can be evaluated as

$$C_1 = \frac{C_{AW}}{\ln(R_i/R_o)}, \quad C_2 = -C_{AW}\frac{\ln R_o}{\ln(R_i/R_o)} \tag{14}$$

The mass flux at the cylinder surface can now be evaluated as

$$N_{AR}|_{r=R_i} = -D_{AB}\left.\frac{\partial C_A}{\partial r}\right|_{r=R_i} \tag{15}$$

The mass-transfer coefficient and the Sherwood number, based on inner cylinder diameter can now be calculated as

$$Sh_D = \frac{2}{\ln(R_o/R_i)} \tag{16}$$

It can be shown for the same boundary conditions that the Sherwood number based on the hydraulic diameter

$$Sh_{Dh} = \frac{k_c(2d)}{D_{AB}} \tag{17}$$

is for the limiting case is given by

$$Sh_{Dh} = \frac{2}{\ln(R_o/R_i)}\left(\frac{2d}{D_i}\right) \tag{18}$$

The computed variation of Sh_{Dh} with Re_{Dh} for very low rotational speeds is illustrated in Figure 11a for the base case. Here, the speed is varied down to a Reynolds number based on the inner cylinder dia. of 0.5. It is indeed seen that as the Reynolds number is reduced, a limiting value of Sh_{Dh} is reached. The numerically obtained limiting values are com-

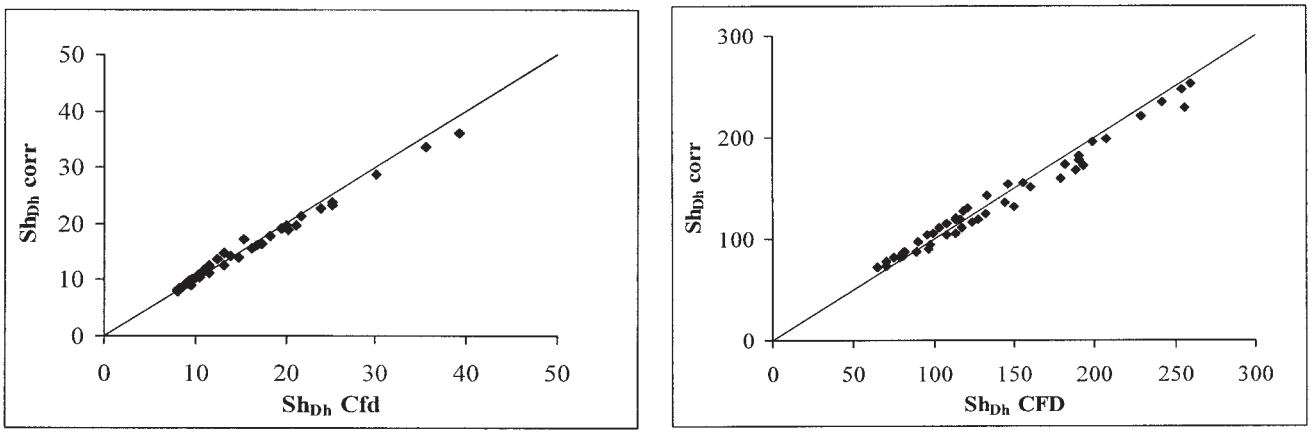

Figure 12. Comparison between the Sherwood number correlation and CFD data for (a) *Couette flow* region, and (b) *Taylor flow* region.

pared in Figure 11b, with that obtained from Eq. 18 earlier for different radius ratios. As expected, the *Sh* (based on the hydraulic diameter) decreases as the radius ratio increases. However, there is a factor of three difference between the predictions and that given by the theoretical expression. Part of this may be attributed to the discrepancy in the definition of the Sherwood number. In the theory, it is based on the concentration difference between the wall and the bulk value, which is taken to be zero. In the CFD simulations, the bulk concentration is based on the cup mean value and takes account of velocity and concentration profiles. The corresponding limiting *Sh* values are shown in Figure 11b with filled squares. The limiting *Sh* values obtained by taking the mass fraction value at the outer radius as the bulk concentration are shown here as open squares. It can be seen that these show a much closer agreement with the theoretical value for a stationary cylinder. The discrepancy that lies between the two, even with a consistent definition of the Sherwood number, may be attributed to the fact that the limiting case considered here is that of a rotating cylinder instead of a translating cylinder for which Eq. 18 is applicable. From a practical point of view, a Sherwood number definition based on the cup mean value is more useful, and the limiting value is taken as

$$Sh_{\lim} = \frac{12}{\ln(R_o/R_i)}\frac{d}{D_i} \tag{19}$$

Using the numerical "data" obtained from the CFD simulations, the following correlations for the Sherwood number have been developed for the *Couette flow* and the *Taylor flow* regimes

$$Sh_{Dh} = \frac{12}{\ln(R_o/R_i)}\frac{d}{D_i} + 0.0048 Re_{Dh} Sc^{1/3}\left[\frac{D_i}{D_o}\right]^{-1.25} \tag{20}$$

$$Sh_{Dh} = \frac{12}{\ln(R_o/R_i)}\frac{d}{D_i} + 0.46 Re_{Dh}^{1/2} Sc^{1/3}\left[\frac{D_i}{D_o}\right]^{-0.1} \tag{21}$$

Using the theoretical analysis of DiPrima et al.,[24] the following correlation is developed to determine the critical Taylor number at which the transition to Taylor vortex regime occurs

$$Ta_{crit} = \frac{1555}{\eta^{1.05}} \tag{22}$$

If the Taylor number for a given situation is less than Ta_{crit}, then the *Couette flow* correlation, that is, Eq. 20, is used to determine Sherwood number. Otherwise, the *Taylor flow* correlation, that is, Eq. 21, is used. The range of parameters for these correlations to be valid is

$$0.3 < \eta < 0.7$$

$$1 < Re_D < 2000$$

$$1 < Sc < 50000$$

A comparison between the Sherwood number correlation (Eq. 20 and Eq. 21), and the CFD data on which it is based is given in Figure 12a (*Couette flow* region) and Figure 12b (*Taylor flow* region) which shows, not surprisingly, very good agreement (within ten percent error) between the two over the range of parameters. The predictions of the correlation with the experimental data of Holman and Ashar[8] is shown in Figures 13a and 13b for benzoic acid-water and benzoic acid-glycerol systems, respectively. It should be noted that Holman and Ashar[8] use a rather high value of *Sc* of 10,000 for the first system; this has been adjusted to a more representative value of 877 (which agrees with the estimates of Bennett and Lewis,[1] Marangosis and Johnson[6] and Tripathi et al[25] among others) in the computation of the experimental *Sh* in Figure 13a. The reported *Sc* of 43,200 for the second system is in agreement with data reported for aqueous glycerol solutions of different concentrations, and the same value of *Sc* is used in the comparison in Figure 13b. Calculations using Eq. 22 show that

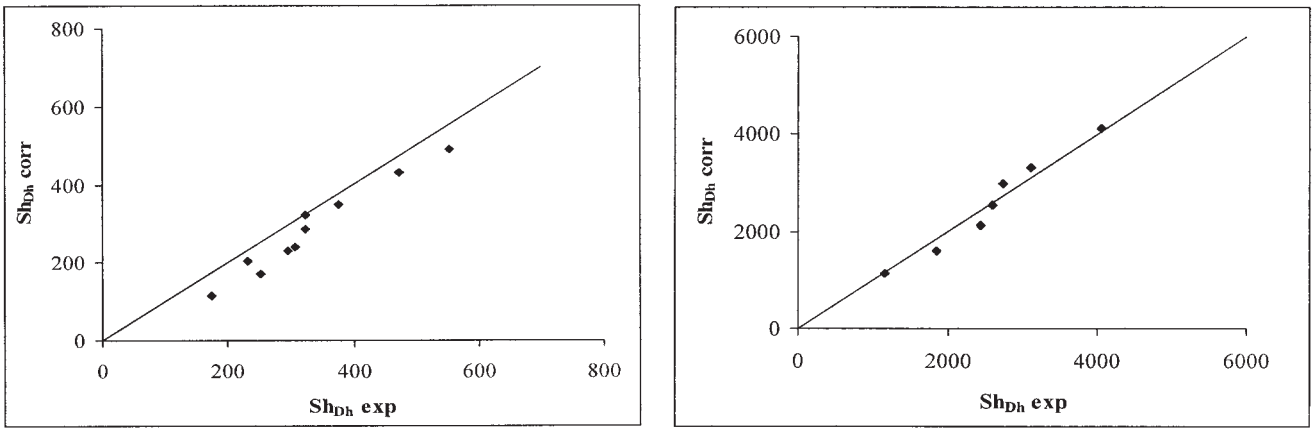

Figure 13. Predictions of the correlation with the experimental data of Holman and Ashar[8] for (a) benzoic acid—water, and (b) benzoic acid-glycerol systems.

these data lie in the Taylor flow regime. Although there is some scatter, there is good qualitative and quantitative agreement between the correlation and the data for both the systems.

Conclusions

CFD simulations are done for the case of a cylinder rotating inside a stationary cylindrical outer vessel filled with liquid. The parameters covered a range of Re, Sc, L/D ratio and radius ratio. The results confirm that the circumferential velocity profile is a strong function of Re and varies from a nearly Couette-type flow at very low Reynolds number to a boundary layer like profile at high Reynolds number. The onset of Taylor vortices has a strong effect on the flow field and the mass transfer mode. Results show that Sherwood number has a linear dependence on the Reynolds number in the Couette-flow regime, and has linear dependence after the onset of Taylor vortices. A correlation based on two regions in the flow field for the Sherwood number has been developed in the parameter range $0.3 < \eta < 0.7$, $1 < Re_D < 2000$ and $1 < Sc < 50{,}000$. Good agreement was found between the experimental and proposed correlation.

Acknowledgment

The calculations reported here have been done using the computational facilities of the CFD Centre, IIT-Madras, India.

Notation

C_A = bulk mean concentration at time t
C_{AW} = solubility concentration of the solid in liquid
d = gap width
D = cylinder dia.
D_{AB} = kinematic diffusivity
i, o = inner and outer cylinder
j_A = average-mass flux
L = cylinder height
k_c = mass-transfer coefficient
N_{AR} = mass flux
r = radial distance from the wall of the inner cylinder
R = cylinder radius, m
Re_{crit} = critical Reynolds number, $\Omega R_i d/\nu$
Re_D = Reynolds number based on inner cylinder dia., $\Omega R_i D_i/\nu$
Re_{Dh} = Reynolds number based on hydraulic dia., $\Omega R_i(2d)/\nu$
S = surface area of the solid
Sc = Schmidt number, ν/D_{AB}
Sh_D = Sherwood number based on inner cylinder diameter, $k_c D_i/D_{AB}$
Sh_{Dh} = Sherwood number based on hydraulic diameter, $k_c(2d)/D_{AB}$
Sh_{lim} = Sherwood number limiting, $12(d/D_i)/[\ln(R_o/R_i)]$
t = time
Ta_{crit} = critical Taylor number, $2(1-\eta)Re^2/(1+\eta)$
u, v, w = velocity components
V = volume of the liquid
W_{tip} = surface speed of the inner cylinder, ΩR_i
Y_A = mass fraction
Y_c = cup mean mass fraction
Y^* = imposed wall mass fraction

Greek letters

Ω = angular velocity (in radians per second)
ρ = density
ν = kinematic viscosity
Γ_{AB} = molecular diffusivity
η = radius ratio, R_i/R_o

Literature Cited

1. Bennett JAR, Lewis JB. Dissolution rates of solids in mercury and aqueous liquids: the development of a new type of rotating dissolution cell. *AIChEJ.* 1958;4(4):418–422.
2. Gabe DR, Robinson DJ. Mass transfer in a rotating cylinder cell—I: laminar flow. *Electrochimica Acta.* 1972;17:1121–1127.
3. Eisenberg M, Tobias CW, Wilke CR. Mass transfer at rotating cylinders. *Chem Eng Prog Symp Ser.* 1955;51(16):1.
4. Johnson AI, Huang CJ. Mass transfer studies in an agitated vessel. *AIChEJ.* 1956;2(3):412–419.
5. Sherwood TK, Ryan JM. Mass transfer to a turbulent fluid with and without chemical reaction. *Chem Eng Sci.* 1959;11(2):81–91.
6. Marangozis J, Johnson AI. A correlation of mass transfer data of solid liquid systems in agitated vessels. *Can J Chem Eng.* 1962;231–237.
7. Pangarkar VG, Yawalkar AA, Sharma MM, Beenackers AACM. Particle-liquid mass transfer coefficient in two/three phase stirred tank reactors. *Ind Eng Chem Res.* 2002;41:4141–4167.
8. Holman KL, Ashar ST. Mass transfer in concentric rotating cylinders with surface chemical reaction in the presence of taylor vortexes. *Chem Eng Sci.* 1971;26:1817–1831.
9. Kataoka K, Doi H, Komai T. Heat/mass transfer in taylor vortex flow with constant axial flow rates. *Int J Heaet Mass Transfer.* 1977;20: 57–63.
10. Legrand J, Dumargue P, Coeuret F. Overall mass transfer to the

rotating inner electrode of a concentric cylindrical reactor with axial flow. *Electrochimica Acta.* 1980;25:669–673.
11. Coeuret F, Legand J. Mass transfer at the electrodes of concentric cylindrical reactors combining axial flow and rotation of the inner cylinder. *Electrochimica Acta.* 1981;26(7):865–872.
12. Grifoll J, Farriol X, Giralt F. Mass transfer at smooth and rough surfaces in a circular couette flow. *Int J Heat Mass Transfer.* 1986; 29(12):1911–1918.
13. Kawase Y, Ulbrecht JJ. Laminar mass transfer between concentric rotating cylinders in the presence of taylor vortices. *Electrochimica Acta.* 1988;33(2):199–203.
14. Holeschovsky UB, Cooney CL. Quantitative description of ultrafiltration in a rotation filtration device. *AIChE J.* 1991;37:1219–1226.
15. Baier G, Grateful TM, Graham MD, Lightfoot EN. Prediction of mass transfer rates in spatially periodic flows. *Chem Eng Sci.* 1999;54:343–355.
16. Taylor GI. Stability of a viscous liquid contained between two rotating cylinders. *Philos Trans Roy Soc London.* 1923;A223:289.
17. Schlichting H. Boundary-layer theory (6th edition). New York: McGraw-Hill; 1968.
18. Jayanti S. Hydrodynamics of jet mixing in vessels. *Chem Eng Sci.* 2001;56:193–210.
19. Rhie CM, Chow WL. Numerical study of the turbulent flow past an airfoil with trailing edge separation. *A I A A J.* 1983;21:1527–1532.
20. Patankar SV. Numerical heat transfer and fluid flow. New York: Hemisphere Publishing; 1980.
21. Leonard BP. A stable and accurate modeling procedure based on quadratic upstream interpolation. *Comp Methods Appl Mech Eng.* 1979;19:59–98.
22. Hirsch C. Numerical computation of internal and external flows. England: John Wiley & Sons, Inc.; 1990.
23. Jones CA. The transition to wavy taylor vortices. *J Fluid Mech.* 1984;157:135–139.
24. DiPrima RC, Eagles PM, Ng BS. The effect of radius ratio on the stability of couette flow and taylor vortex flow. *Phys Fluids.* 1984; 27(10):2403–2411.
25. Tripathi G, Singh SK, Upadhay SN. Mass transfer at rotating cylinders. *Indian J Tech.* 1971;9:237–241.
26. Bird RB, Stewart WE, Lightfoot EN. Transport phenomena. New York: Wiley, 1960.

Manuscript received Oct. 26, 2004, and revision received Mar. 9, 2005.